

RSC Advances



This is an *Accepted Manuscript*, which has been through the Royal Society of Chemistry peer review process and has been accepted for publication.

Accepted Manuscripts are published online shortly after acceptance, before technical editing, formatting and proof reading. Using this free service, authors can make their results available to the community, in citable form, before we publish the edited article. This *Accepted Manuscript* will be replaced by the edited, formatted and paginated article as soon as this is available.

You can find more information about *Accepted Manuscripts* in the [Information for Authors](#).

Please note that technical editing may introduce minor changes to the text and/or graphics, which may alter content. The journal's standard [Terms & Conditions](#) and the [Ethical guidelines](#) still apply. In no event shall the Royal Society of Chemistry be held responsible for any errors or omissions in this *Accepted Manuscript* or any consequences arising from the use of any information it contains.

ARTICLE

Synthesis of Yolk/Shell Fe₃O₄@Poly(ionic liquid)s-Derived Nitrogen doped Graphitic Porous Carbon Materials and Its Application as Support for Nickel Catalysts

Cite this: DOI: 10.1039/x0xx00000x

Received 00th January 2012,
Accepted 00th January 2012

DOI: 10.1039/x0xx00000x

www.rsc.org/

Mohammad Reza Nabid*, Yasamin Bide, Zahra Habibi

The synthesis of yolk/shell spheres including a movable magnetic core, a poly(ionic liquid)s-derived porous carbon shell, and nickel nanoparticles confined within the porous shell is reported. The as-prepared carbon shell is graphitic, and porous, as proven by x-ray diffraction, Brunauer–Emmett–Teller equation, and transmission electron microscopy characterizations. The ensuing catalyst has been employed for the tandem dehydrogenation of sodium borohydride and hydrogenation of several nitro/nitrile compounds in aqueous media which resulted high yields with a very low amount of the catalyst.

Introduction

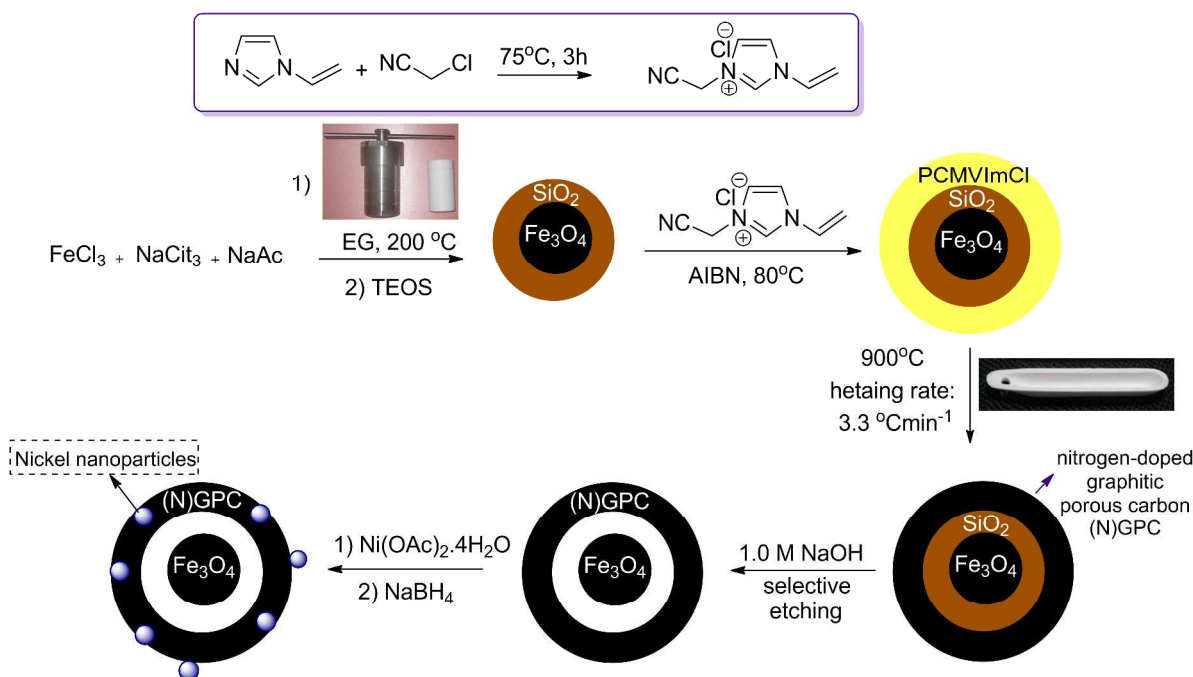
Due to their unique properties, such as large surface area, multifunctionality and excellent loading capacity, yolk/shell nanostructures (YSNs) consisting of a core encapsulated in a hollow capsule with a porous shell have attracted considerable attention over the past few years in a variety of applications including catalysis, storage, and drug delivery.^{1–4} Among them, YSNs with a magnetic core, due to the improving the stability, biocompatibility, and significant magnetization strength of iron oxides are desirable in biomedical applications.^{5, 6} Also YSNs with a magnetic core and a functional shell are attractive because of their potential applications as catalyst supports and eliminating time-consuming separation procedures such as filtration or centrifugation. On the other hand, the outer shell of yolk-shell composites is usually needed to have both high surface areas and good dispersion characteristics to be a catalyst support. Among the supports, carbon materials due to the electronic and heat conductivity, chemical and physical stability, its sustainable nature and the possibility of control of its chemical connectivity and nanostructure are attractive choices.⁷ In contrast to disordered or amorphous carbon, graphitized carbons with the well-developed crystalline structure present high electric conductivity and enhanced chemical stability.^{8–10} Therefore, from the viewpoint of the catalytic application, graphitized mesoporous carbons with relatively large surface area and high crystallinity are more desired. Because of totally evaporation or decomposition of most carbon containing organic compounds to gaseous products during high-temperature carbonization process, currently only a few conventional carbon-containing sources are used as carbonaceous precursors. The synthesis of N-doped carbon materials has been mainly accomplished under harsh reaction

conditions, such as post treatment with amines or urea,¹¹ ammonia,¹² or direct methods employing polyaniline¹³ or acetonitrile.¹⁴ In recent years, porous carbons were also obtained *via* the hydrothermal carbonization of biomass derivatives.^{15,16} Employing suitable natural precursors led to the synthesis of nitrogen-doped carbons.¹⁷ In 2010, Paraknowitsch and coworkers employed ionic liquids (ILs) for the synthesis of mesoporous N-doped graphitic carbon at 1000°C in a SBA-15 template.¹⁸ Using ILs and poly(ionic liquid)s (PILs) as the precursors for synthesis of carbon materials leads to a feasible synthesis with controlling the structure on different length scales, and also the incorporation of a certain amount of heteroatoms. The most advantage of them compared with other carbon precursors is their charged nature, which cause a negligible vapor pressure, even at elevated temperatures where typical carbonization occurs. So, high carbon yields under control of process and morphology can be obtained. ILs and PILs molecules due to a clever choice of anion and cation and the overall hydrophobicity can wet most surfaces and form very homogeneous films and coatings.¹⁹ Furthermore, ILs and PILs contain firmly incorporated conjugated nitrogen, sulfur, boron, or phosphorus atoms to provide a stable and delocalized charge which many of these heteroatoms stay incorporated within the carbonaceous scaffolds, consequently creating heteroatom doped carbons. The doping with nitrogen atoms enhances the electric conductivity and catalytic activity.^{20–22} Moreover, metal or metal oxide nanoparticles can be stabilized in nitrogen doped carbon framework through the generation of topological defects and the activation of nitrogen-neighboring carbon atoms.^{23, 24} Due to the additional backbone immobilization, higher carbon yields have been observed in the case of PILs.^{25–28} Very recently, PILs have gained much attention as novel carbon precursors.^{18, 26–30}

Due to our interest in the development of catalysts for useful new synthetic methodologies,³¹⁻³⁶ as well as the general importance of this issue, herein, we report the synthesis and characterization of yolk/shell $\text{Fe}_3\text{O}_4@$ Poly(ionic liquid)-derived nitrogen doped graphitic porous carbon materials, and its application as support for nickel catalysts was also examined. Recently, we reported a catalyst for dehydrogenation of sodium borohydride and hydrogenation of nitriles.³⁷ In this work, the as-prepared catalyst was employed for tandem dehydrogenation of sodium borohydride and hydrogenation of several nitro/nitrile compounds. We chose nickel nanoparticles, because employing the first row transition metals as catalysts in the reduction reactions is much more desired than the precious metals owing to the important advantages such as cheapness and earth abundance.³⁸⁻⁴¹

Results and discussion

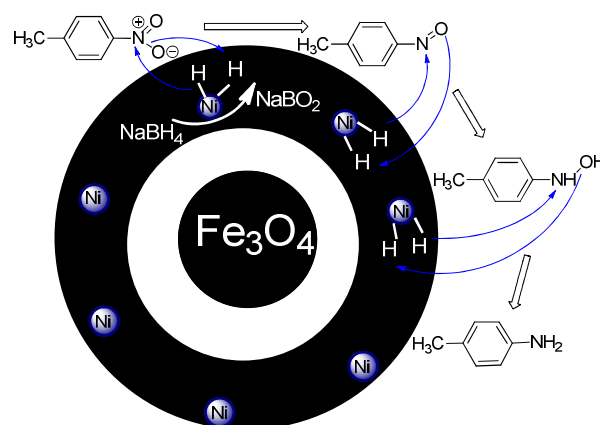
$\text{Fe}_3\text{O}_4@$ SiO_2 particles were synthesized with a modified solvothermal reaction, followed by a sol-gel process. Then, the poly(3-cyanomethyl-1-vinylimidazolium chloride) (PCMVImCl) layer was coated on the as prepared particles via polymerization of IL monomer in ethanol. Pyrolysis of $\text{Fe}_3\text{O}_4@$ $\text{SiO}_2@$ poly(imidazolium-based)ILs, allowed preparation of magnetic nitrogen-doped graphitic porous carbon ((N)-GPC) materials in general. Then, SiO_2 middle layer was removed by selective etching process to obtain hollow structures. Finally, nickel nanoparticles immobilized on YS $\text{Fe}_3\text{O}_4@$ PIL-d(N)GPC were synthesized by introducing Ni^{2+} ions which have good interaction their reduction with sodium borohydride (Scheme 1).



Scheme 1 Schematic diagram of the synthesis of NiNPs@YS $\text{Fe}_3\text{O}_4@$ PIL-d(N)GPC.

Moreover, the band at 1091 cm^{-1} related to Si-O-Si stretching vibrations of SiO_2 shell can be seen. The adsorption peaks at 3144 and 2926 cm^{-1} can be assigned as the C-H stretching vibrations of the imidazole ring and the alkyl chains.

The supported catalyst was employed for tandem dehydrogenation of sodium borohydride and hydrogenation of nitro/nitrile compounds. A plausible mechanism for this reaction catalyzed by NiNPs@YS $\text{Fe}_3\text{O}_4@$ PIL-d(N)GPC has been shown in Scheme 2. The chemical modification of the adsorbent surface with nitrogen based functional groups or other heteroatom doping and transition metal doping increase the binding energy states of H_2 .⁴² On the other hand, in aqueous media the organic substrates are concentrated on the hydrophobic pores of graphitic porous carbon. In our catalytic system, these three issues are combined; substrates, H_2 and catalyst are in hydrophobic pores of graphitic porous carbon, so it is expected that an efficient catalytic reaction would achieve. Fourier transform Infrared (FT-IR) spectra of Fe_3O_4 magnetic particles, and $\text{Fe}_3\text{O}_4@$ SiO_2 were given in Fig. S1. Figure 1A-C show FT-IR spectra of $\text{Fe}_3\text{O}_4@$ $\text{SiO}_2@$ PCMVImCl, $\text{Fe}_3\text{O}_4@$ $\text{SiO}_2@$ PIL-d(N)GPC, and YS $\text{Fe}_3\text{O}_4@$ PIL-d(N)GPC, respectively. FT-IR spectrum of $\text{Fe}_3\text{O}_4@$ $\text{SiO}_2@$ PCMVImCl (Fig. 1A) shows absorption bands at 576 cm^{-1} and 3431 cm^{-1} ascribed to the Fe-O vibrating and O-H vibrating, respectively.



Scheme 2 A plausible mechanism for the tandem dehydrogenation of sodium borohydride and reduction of 4-nitrotoluene catalyzed by NiNPs@YS Fe₃O₄@PIL-d-(N)GPC.

The stretching vibrations belonging to the C–N of the imidazole rings would be appeared at 1138 cm⁻¹ but it was overlapped with the band at 1091 cm⁻¹ related to Si–O–Si. The peak at about 1633 cm⁻¹ is related to the C=N stretching vibration of the imidazole ring. FT-IR spectrum of Fe₃O₄@SiO₂@PIL-d-(N)GPC is given in Figure 1B. The weak band at 3442 cm⁻¹ can be attributed to the N–H symmetric stretching vibration.⁴³ The band at 2925 cm⁻¹ displays the C–H stretching vibration. The broad peak around 1259 cm⁻¹ is related to the C–N stretching vibration which overlapped with the peak of Si–O–Si in FT-IR spectrum of Fe₃O₄@SiO₂@PIL-d-(N)GPC, but observable in the spectrum of YS Fe₃O₄@PIL-d-(N)GPC.⁴⁴ Therefore, the FT-IR analysis confirms the presence of N-H and C-N species in the ensuing porous carbon. In FT-IR spectrum of YS Fe₃O₄@PIL-d-(N)GPC (Fig. 1C), the adsorption peak of Si–O–Si at 1099 cm⁻¹ was removed which confirmed the successful elimination of the middle SiO₂ layer.

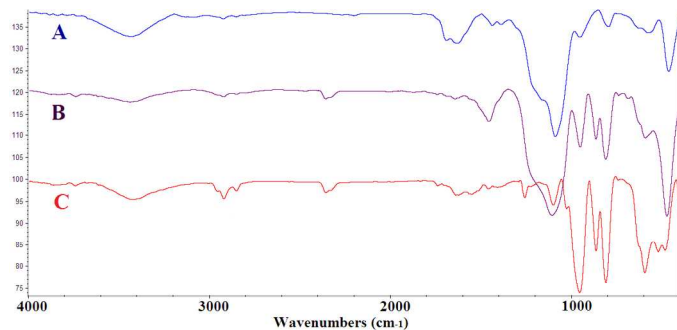


Fig. 1 FT-IR spectra of Fe₃O₄@SiO₂@PCMVIImCl (A), Fe₃O₄@SiO₂@PIL-d-(N)GPC (B), and YS Fe₃O₄@PIL-d-(N)GPC (C)

The XRD spectra of Fe₃O₄@SiO₂ and Fe₃O₄@SiO₂@PCMVIImCl have been presented in Fig. S2. In the XRD pattern of Fe₃O₄@SiO₂@PIL-d-(N)GPC (Fig. 2A), besides the characteristic diffraction peaks of Fe₃O₄ at $2\theta = 32.14^\circ$, 35.57° , 51.34° and a broad peak at around $2\theta = 20.12^\circ$ correspond to SiO₂, the wide diffraction peak at around $2\theta = 25.63^\circ$ is observed which related to the (002) plane of graphitic mesoporous carbon, respectively. In the XRD pattern of the YS Fe₃O₄@PIL-d-(N)GPC (Fig. 2B), as expected due to the removing of silica intermediate shell, the peak of silica at 20.12° is eliminated.

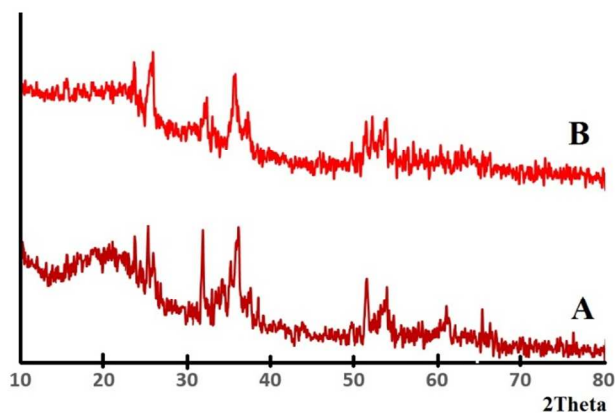


Fig. 2 XRD patterns of Fe₃O₄@PIL-d-(N)GPC (A) and YS Fe₃O₄@PIL-d-(N)GPC (B).

Figure 3A-C shows the thermograms (TGs) of three samples: Fe₃O₄, Fe₃O₄@SiO₂, and Fe₃O₄@SiO₂@PCMVIImCl, respectively. Compared with the TGA diagram of Fe₃O₄@SiO₂ particles, the much higher weight loss observed in the TGA diagram of Fe₃O₄@SiO₂@PCMVIImCl originates from the organic composition of the composites. Before thermal decomposition a slight weight loss of around 5.2%, as shown in Fig. 3C, is probably due to the evaporation of physically absorbed moisture, and this value is a little higher in the Fe₃O₄@SiO₂@PCMVIImCl composite particles compared to Fe₃O₄@SiO₂, which is caused by the high hydrophilicity of the PCMVIImCl shell. Fe₃O₄@SiO₂ clearly shows two types of distinct weight loss events: successive rapid decompositions at 140 °C and 260 °C due to the decomposition of the organic shell vs. the relatively slow weight loss region at around 520–700 °C due to the intermolecular condensation of the silica particles. The weight retention obtained for Fe₃O₄@SiO₂@PCMVIImCl (Fig. 3C) at 780 °C is 62.9%. Using the weight retention at 780 °C obtained for Fe₃O₄@SiO₂ (91.2%) as a reference, the PCMVIImCl weight content is calculated to be 28.3%. Two rapid thermal degradation events of Fe₃O₄@SiO₂@PCMVIImCl occur at 283, and 374 °C under air atmosphere, which are due to the cleavage of the PCMVIImCl polymer backbone (or carbonation).

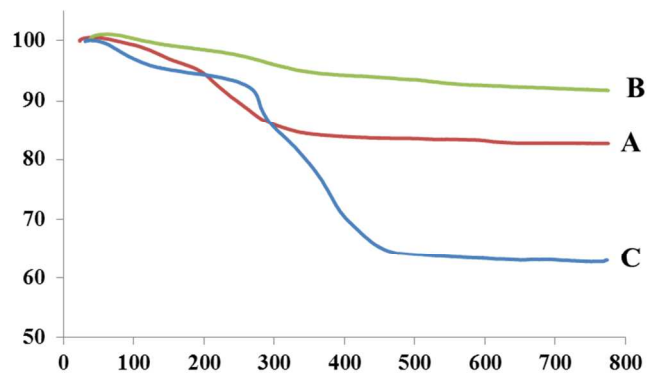


Fig. 3 TGA curves of Fe₃O₄@SiO₂ (A), and Fe₃O₄@SiO₂@PCMVIImCl (B).

The TEM image of YS Fe₃O₄@PIL-d-(N)GPC is presented in Figure 4A which shows Fe₃O₄ magnetic particles coated with a folded, lamellar-like morphology of stiff graphite plates with the curved and wrapped structure. As clearly revealed, the

lamellar-like structures are in fact layered graphitic nanostructures. Figure 5 shows TEM images of NiNPs@YS Fe₃O₄@PIL-d(N)GPC which three distinct components, the black cores of Fe₃O₄, the grey shells of graphite plates and the small black spheres of nickel nanoparticles are observed.

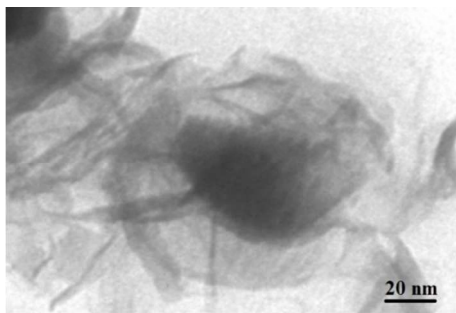


Fig. 4 TEM image of YS Fe₃O₄@PIL-d(N)GPC.

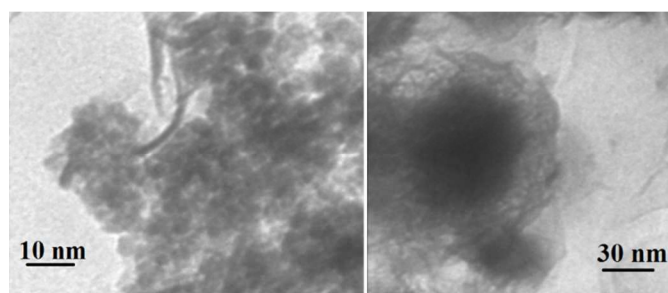


Fig. 5 TEM images of NiNPs@YS Fe₃O₄@PIL-d(N)GPC.

The XPS spectrum of NiNPs@YS Fe₃O₄@PIL-d(N)GPC possesses four peaks centered at 284.7, 400.1, 530.9, and 711.4 eV, corresponding to C 1s, N 1s, O 1s, and Fe 2p respectively (Fig. 6). The oxygen mainly arises from Fe₃O₄ and the thermally stable groups in the carbon except for that of oxygen or water absorbed on the carbon surface. The high-resolution XPS of N 1s in the NiNPs@YS Fe₃O₄@PIL-d(N)GPC demonstrates two peaks of N1s at 398.7 eV and 401.3 eV attributed to pyridinic and quaternary nitrogen in carbon structure, respectively (Figure 7A). These two different binding energies shows that nitrogen is embedded into the graphitic carbon structure mainly in two forms.⁴⁵ The spectrum of the Ni2p core level of NiNPs@YS Fe₃O₄@PIL-d(N)GPC is shown in Figure 7B, which demonstrates two bands at 855.9 and 873.5 eV assigned to Ni⁰2p_{3/2} and Ni⁰2p_{1/2}, respectively. The two peaks with lower intensities at 861.7 and 879.5 eV corresponded to Ni²⁺ species that could have been formed during the XPS sample preparation due to the sensitivity of the stabilized Ni(0) nanoclusters to the aerobic atmosphere. The Ni loading for the sample used for XPS measurements was 9.8 wt%. Moreover, the absence of silicon band at around 104 eV confirms the selective etching of silica shell.

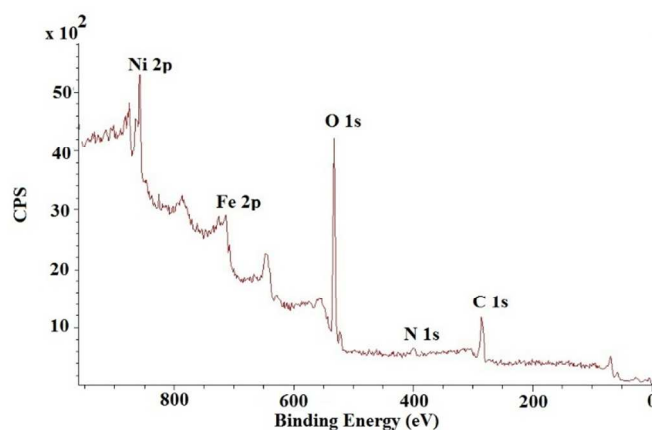


Fig. 6 XPS full spectrum of NiNPs@YS Fe₃O₄@PIL-d(N)GPC.

Figure 8 shows the nitrogen adsorption–desorption isotherms recorded from YS Fe₃O₄@PIL-d(N)GPC. The results showed that the average pore sizes are 2.5 nm and by applying the BET model, the total surface area is calculated to be 138.63 m²g⁻¹. BET testing also showed a pore structure consisting of micropores, and mesopores. The pore size distribution curve has been shown in Fig. S3.

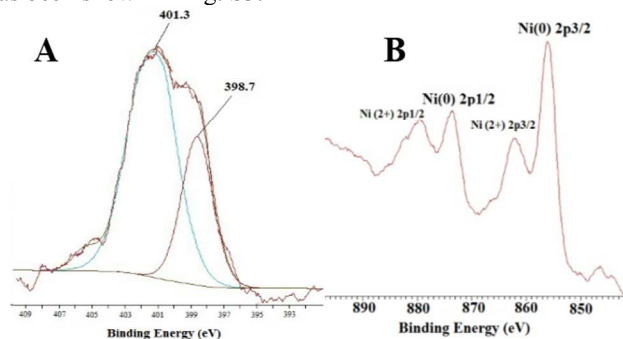


Fig. 7 XPS high-resolution spectra of the N 1s (A) and Ni 2p (B) of the as-prepared NiNPs@YS Fe₃O₄@PIL-d(N)GPC.

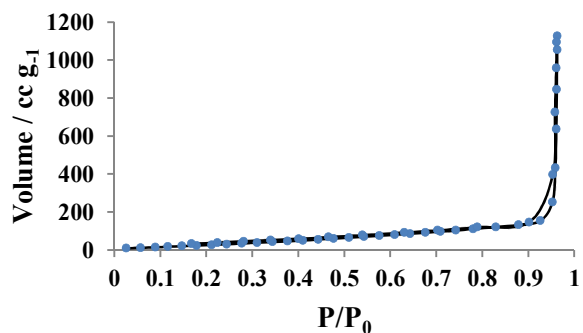


Fig. 8 Nitrogen sorption isotherms of YS Fe₃O₄@PIL-d(N)GPC.

Catalytic hydrolysis of sodium borohydride can generate 4 mol of hydrogen per mol of sodium borohydride at room temperature, which making itself a useful approach for hydrogen release from sodium borohydride (hydrogen content of 10.7 wt %).⁴⁶

On the other hand, theoretical and also experimental studies have established that substitutional doping of carbon materials can be employed to modify their physical and/or chemical properties and also affect the hydrogen adsorption and desorption process.⁴⁷ A modification approach of bases activation,^{48,49} (N-doped structure), transition-metal catalysts,^{46,48} (NiNPs), and nanoscaffolds^{46,51} by NiNPs@YS Fe₃O₄@PIL-d-(N)GPC allows sodium borohydride to release 4 mol of H₂ in aqueous solution at room temperatures.

Our investigation on the catalyst loading showed a high atom efficiency of title NiNPs@YS Fe₃O₄@PIL-d-(N)GPC. We first used 4-nitrotoluene as a model compound to demonstrate NiNPs@YS Fe₃O₄@PIL-d-(N)GPC catalysis for the tandem dehydrogenation of sodium borohydride and hydrogenation of nitro compounds and to obtain the optimum reaction conditions. We examined the catalytic reactions at room temperature in different solvents including DMSO, methanol, ethanol, water, and found water to be the best solvent to convert 4-nitrotoluene to p-toluidine. Actually, because of the hydrophobic nature of porous carbon, the reactants tend to collect at those sites rather than water solvent. On the other hand, nickel nanoparticles as catalyst and hydrogen also exist in the pores. So, as the reagents and catalyst concentrate in an area, probably an efficient catalytic reaction occurs. Moreover, to optimize the amount of the catalyst, different amounts of the catalyst including 0.8, 1, and 1.2 mol% Ni were used for model reaction in water at room temperature. The optimum amount of the catalyst considering the reaction time and yield was 1 mol%. In addition, the model reaction was carried out without catalyst which no product was obtained over 24 h. According to these results, the optimum reaction condition is water as solvent and 1 mol% Ni for the NiNPs@YS Fe₃O₄@PIL-d-(N)GPC to

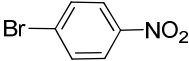
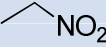
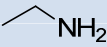
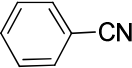
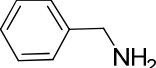
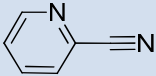
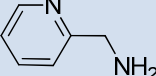
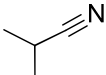
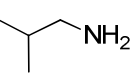
catalyze the tandem reaction. The summary of these results were given in Table S1.

We also studied the support effect on nickel nanoparticles catalysis. Nickel nanoparticles were used without a support in model reaction which were active catalysts for catalytic reduction of 4-nitrotoluene, but the conversion yield was low (33%). It could be due to aggregation of nickel nanoparticles without a support and subsequently reduced catalytic activity. Moreover, the improvement of the results, in comparison with nickel nanoparticles could be due to π - π interactions of the aromatic groups in reactants with the support preferring the close proximity of the reagents to the catalytic sites.

Then, to evaluate the general applicability of the catalyst, different nitro compounds were tested for reduction reaction using sodium borohydride and 0.006 g catalyst containing 1 mol % Ni at 25°C in water (Table 1) which ¹H NMR spectra of the products have been presented in Fig. S4-10. As can be seen, various nitro compounds can generate the related amine in excellent yields. The catalytic reaction could be extended to 1-methoxy-4-nitrobenzene, 1-nitronaphthalene, 1-fluoro-4-nitrobenzene, 1-iodo-3-nitrobenzene, 1-bromo-4-nitrobenzene, and also nitroethane compounds, which were all transformed to the respective amine derivatives with high yields (Table 1, entries 2–7). Moreover, with respect to general applicability of the catalyst NiNPs@YS Fe₃O₄@PIL-d-(N)GPC, we also tested reduction reaction of nitrile compounds to the corresponding amines which the results were shown in Table 1, entries 8-10. The reduction of benzonitriles is an important issue, since allows the easy preparation of a variety of biologically active benzyl amines compounds. Moreover, the reduction reaction of picolinonitrile was examined which resulted the related amine in high yield (Table 1, entry 9). The ¹H NMR spectra of the products have been given in Fig. S11-13.

Table 1 The reduction reaction of nitro/nitrile compounds with NiNPs@YS Fe₃O₄@PIL-d-(N)GPC as catalyst.^a

Entry	Compound	Product	Time (min)	Isolated yield (%)
1			30	90
2			30	91
3			30	87
4			25	92
5			30	90

6			30	90
7			30	88
8			60	89
9			60	80
10			45	87

^a Reaction conditions: 5 mL of deionized water, 1 mmol nitro/nitrile, 0.5 mmol NaBH₄, and 0.006 g catalyst at 25°C.

As the catalysis is a kinetic phenomenon, to investigate the recyclability and deactivation of the catalyst, the initial rates obtained from kinetic plots should be considered. If a single data point after long reaction time in each run was taken, one might incorrectly conclude that the catalyst is completely stable and recyclable.⁵² Therefore, the conversion yields for every run after 10 min for reduction reaction of 4-nitrotoluene were measured (Fig. 9A). As the conversion yields after 10 min for seven runs didn't reduce considerably, we may conclude the good stability and recyclability of the synthesized catalyst. To examine the productivity of the as prepared catalyst, we investigated the reduction reaction of 4-nitrotoluene as a model reaction up to seven cycles after completion of the reaction. By design, the magnetic extraction excludes the need for filtration or centrifugation and the workup of the final reaction mixture to recover the catalyst and consequently allows for easy recycling of the catalyst. The results have been presented in Fig. 9B which indicated that the yield of product after every run does not change significantly.

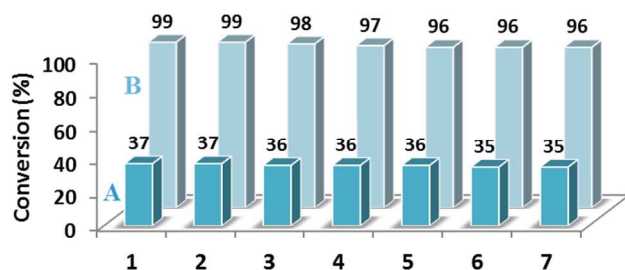


Fig. 9 Effect of recycling on the catalytic activity and productivity of NiNPs@YS Fe₃O₄@PIL-d-(N)GPC after 10 (A) and after 30 min (B).

Conclusion

In this work, we have attained several important approaches: i) Having a heterogeneous catalyst with the advantage of being efficient, reusable, cost-effective and also removing the need of

the catalyst filtration with magnetically separating; ii) Having a yolk shell structure with unique properties such as large surface area, multi-functionality and excellent loading capacity; iii) Employing porous carbon as stabilizer for nanoparticles which have several important advantages such as large surface area, stability, and straightforward synthesis; iii) Using poly(ionic liquid)s as precursor for synthesis of nitrogen doped porous carbon; iv) Carrying out the tandem reaction in an environmentally friendly and safe method; v) Having the catalytic activity for reduction of nitro and nitrile compounds with high yields.

Experimental

Materials

1-Vinylimidazole, and chloroacetonitrile were obtained from Sigma-Aldrich and used without further purification. 2,2'-Azobis(2-methylpropanitrile) (AIBN) (Aldrich) was recrystallized from methanol. CMVImCl as IL monomer was prepared according to the literature,⁵³ and its ¹H NMR spectrum was presented in Fig. S14. Nickel (II) acetate tetrahydrate was purchased from Alfa Aesar. Ferric chloride hexahydrate (FeCl₃·6H₂O), trisodium citrate dehydrate (Na₃Cit·2H₂O), sodium acetate (NaAc), ethylene glycol (EG), tetraethyl orthosilicate (TEOS), and sodium hydroxide (NaOH) were purchased from Merck Chem. Toluene was dried from sodium. Dichloromethane and methanol were dried from calcium hydride and magnesium respectively. All other solvents and reagents were purchased from Aldrich or Merck and used without further purification unless otherwise stated.

Instruments and characterization

IR spectra were recorded on a Bomem MB-Series FT-IR spectrophotometer. Transmission electron microscopy (TEM) analyzes were performed by LEO 912AB electron microscope. Ultrasonic bath (EUROSONIC[®] 4D ultrasound cleaner with a frequency of 50 kHz and an output power of 350 W) was used to disperse materials in solvents. Thermogravimetric analysis (TGA) was carried out using STA 1500 instrument at a heating

rate of 10 °C min⁻¹ in air. The specific surface area was calculated using the Brunauer–Emmett–Teller (BET) equation. Pore size distribution was determined by Barrett–Joyner–Halenda (BJH) method. The samples were degassed at 150 °C for 20 h before measurements. X-ray powder diffraction (XRD) data were collected on an XD-3A diffractometer using Cu K α radiation. XPS analysis was performed using a VG multilab 2000 spectrometer (ThermoVG scientific) in an ultrahigh vacuum. Catalysis products were analyzed using a Varian 3900 gas chromatograph (GC) (conversions were obtained using n-decane as an internal standard). AA-680 Shimadzu (Kyoto, Japan) flame atomic absorption spectrometer (AAS) with a deuterium background corrector was used for determination of the metal. ¹H NMR spectra were recorded with a BRUKER DRX-300 AVANCE spectrometer, and DMSO or CDCl₃ were used as solvents.

Synthesis and coating of Fe₃O₄ with silica (Fe₃O₄@SiO₂)

Fe₃O₄ nanoclusters were synthesized according to the literature.⁵⁴ Typically, FeCl₃ (0.65 g, 4.0 mmol) and trisodium citrate (0.20 g, 0.68 mmol) were first dissolved in ethylene glycol (20 mL). Afterward, NaAc (1.20 g) was added with stirring. The mixture was stirred vigorously for 30 min and then sealed in a Teflon-lined stainless-steel autoclave. The autoclave was heated at 200 °C and maintained for 10 h, and then allowed to cool to room temperature. The obtained Fe₃O₄ particle suspension was washed successively with H₂O and EtOH three times and then dried in a vacuum oven for 12 h at room temperature. For coating of Fe₃O₄ with silica, 50.0 mL as-prepared Fe₃O₄ nanocluster solution (containing 0.4 g Fe₃O₄) was dispersed into the mixture of deionized water (10.0 mL), ethanol (100.0 mL) and NH₃.H₂O (50.0 mL). After ultrasonic for 10 min, a certain amount of TEOS was quickly added into the system. The reaction was allowed to proceed with stirring for 8 h at room temperature. Finally the products were separated by magnet and washed by deionized water for the next-step.

Preparation of Fe₃O₄/SiO₂/PILs composite particles (Fe₃O₄@SiO₂@PCMVIImCl)

The PIL layer on silica particles was synthesized via polymerization of IL monomer in the presence of Fe₃O₄@SiO₂ particles in ethanol. In a general polymerization procedure, 3 g of CMVIImCl monomer, 200 mg of AIBN and 5 mL of deionized water were added to 70 mL of ethanol containing 3 g of dispersed Fe₃O₄@SiO₂ particles. The dispersion was degassed by purging with nitrogen for 30 min prior to polymerization. The polymerization was conducted under vigorous stirring at 80 °C overnight. After cooling down, the obtained Fe₃O₄@SiO₂@PCMVIImCl composite particles were washed by four centrifugation/redispersion cycles with deionized water, and dried at 60 °C under vacuum.

Carbonization process

In a typical experiment, the dried Fe₃O₄@SiO₂@PCMVIImCl sample was put into an aluminum oxide crucible in an oven and heated under a N₂ atmosphere to 900 °C at a heating rate of 3.3 °C min⁻¹. The sample was further kept at 900 °C for 1 h and cooled down slowly to room temperature.

Preparation of the yolk/shell Fe₃O₄@Poly(ionic liquid)s-derived nitrogen-doped graphitic porous carbon materials (YS Fe₃O₄@PIL-d(N)GPC)

Fe₃O₄@Poly(ionic liquid)s-derived nitrogen-doped graphitic porous carbon materials were soaked in 1.0 M NaOH solution under mechanical stirring for 12.0 h; the SiO₂ layer between the carbon shell and the Fe₃O₄ core was selectively etched. After

washed with deionized water and ethanol several times, the black product was dried in oven overnight.

Synthesis of nickel nanoparticles immobilized on YS Fe₃O₄@PIL-d(N)GPC (NiNPs@YS Fe₃O₄@PIL-d(N)GPC)

Aqueous solution of nickel (II) acetate tetrahydrate (0.01 mL, 0.15 M) and YS Fe₃O₄@PIL-d(N)GPC (0.1 g in 10 mL) were mixed and placed in an ultrasonic bath (50 kHz) for 10 min to well disperse metal ions in the hybrid material. Mixture was stirred at room temperature for 8 h and then reduction was carried out with addition of 0.5 mL aqueous solution of NaBH₄ (0.01M) to the mixture and stirring at room temperature for 1 h. It was filtered under vacuum, washed well with ethanol and water (2×20 mL) and dried under vacuum at 50 °C for 4 h to obtain NiNPs@YS Fe₃O₄@PIL-d(N)GPC. The AAS and TGA were used to determine the amount of nickel in the synthesized catalyst.

General procedure for tandem dehydrogenation of sodium borohydride and hydrogenation of nitro/nitrile compounds with NiNPs@YS Fe₃O₄@PIL-d(N)GPC as catalyst

To 2 mL distilled water, 1 mmol nitro/nitrile was added and to this solution 0.006 g ultrasonically dispersed NiNPs@YS Fe₃O₄@PIL-d(N)GPC catalyst (1 mol% Ni) in water (3.0 mL) was introduced. Finally, 0.5 mmol NaBH₄ (0.038 g) was introduced. The mixture was stirred. After the reaction completion, the catalyst was removed via an external magnetic field and washed twice with CH₂Cl₂ (6.0 mL). Then the organic phase was combined and removed the solvent under vacuum to give the pure product. The conversions were determined by the gas chromatography (GC) analysis.

Acknowledgements

The financial support provided by the Iran National Science Foundation (INSF) is gratefully acknowledged.

Notes and references

^a Faculty of Chemistry, Department of Polymer, Shahid Beheshti University, G.C., P.O. Box 1983969411 Tehran, Iran.

Electronic Supplementary Information (ESI) available: [details of any supplementary information available should be included here]. See DOI: 10.1039/b000000x/.

1. R. Güttel, M. Paul and F. Schüth, *Catal. Sci. Tech.*, 2011, **1**, 65-68.
2. C. C. Yec and H. C. Zeng, *Chem. Mater.*, 2012, **24**, 1917-1929.
3. Y. Chen, Y. Gao, H. Chen, D. Zeng, Y. Li, Y. Zheng, F. Li, X. Ji, X. Wang and F. Chen, *Adv. Funct. Mater.*, 2012, **22**, 1586-1597.
4. T. Yang, J. Liu, Y. Zheng, M. J. Monteiro and S. Z. Qiao, *Chem. Eur. J.*, 2013, **19**, 6942-6945.
5. Y. Chen, H. Chen, M. Ma, F. Chen, L. Guo, L. Zhang and J. Shi, *J. Mater. Chem.*, 2011, **21**, 5290-5298.
6. H. Wu, G. Liu, S. Zhang, J. Shi, L. Zhang, Y. Chen, F. Chen and H. Chen, *J. Mater. Chem.*, 2011, **21**, 3037-3045.
7. J. Lee, J. Kim and T. Hyeon, *Adv. Mater.*, 2006, **18**, 2073-2094.

8. J. Zeng, F. Su, Y.-F. Han, Z. Tian, C. K. Poh, Z. Liu, J. Lin, J. Y. Lee and X. Zhao, *J. Phys. Chem. C*, 2008, **112**, 15908-15914.
9. J. Zeng, F. Su, J. Y. Lee, X. Zhao, J. Chen and X. Jiang, *J. Mater. Sci.*, 2007, **42**, 7191-7197.
10. Y. Wang, F. Su, J. Y. Lee and X. Zhao, *Chem. Mater.*, 2006, **18**, 1347-1353.
11. R. Pietrzak, H. Wachowska and P. Nowicki, *Energy & Fuels*, 2006, **20**, 1275-1280.
12. F. Jaouen, M. Lefevre, J. Dodelet and M. Cai, *J. Phys. Chem. B*, 2006, **110**, 5553-5558.
13. L. Li, E. Liu, Y. Yang, H. Shen, Z. Huang and X. Xiang, *Mater. Lett.*, 2010, **64**, 2115-2117.
14. P. Matter, L. Zhang and U. Ozkan, *J. Catal.*, 2006, **239**, 83-96.
15. M. Titirici, R. White, C. Falco and M. Sevilla, *Energy Environ. Sci.*, 2012, **5**, 6796-6822.
16. M. Sevilla and A. Fuertes, *Chem. Eur. J.*, 2009, **15**, 4195-4203.
17. F. Braghiroli, V. Fierro, M. Izquierdo, J. Parmentier, A. Pizzi and A. Celzard, *Carbon*, 2012, **50**, 5411-5420.
18. J. P. Paraknowitsch, J. Zhang, D. Su, A. Thomas and M. Antonietti, *Adv. Mater.*, 2010, **22**, 87-92.
19. M. Antonietti, D. Kuang, B. Smarsly and Y. Zhou, *Angew. Chem. Int. Ed.*, 2004, **43**, 4988-4992.
20. R. Czerw, M. Terrones, J.-C. Charlier, X. Blase, B. Foley, R. Kamalakaran, N. Grobert, H. Terrones, D. Tekleab and P. Ajayan, *Nano Lett.*, 2001, **1**, 457-460.
21. K. K. Datta, V. V. Balasubramanian, K. Ariga, T. Mori and A. Vinu, *Chem. Eur. J.*, 2011, **17**, 3390-3397.
22. K. Gong, F. Du, Z. Xia, M. Durstock and L. Dai, *Science*, 2009, **323**, 760-764.
23. Y.-H. Li, T.-H. Hung and C.-W. Chen, *Carbon*, 2009, **47**, 850-855.
24. A. Zamudio, A. L. Elías, J. A. Rodríguez-Manzo, F. López-Urías, G. Rodríguez-Gattorno, F. Lupo, M. Rühle, D. J. Smith, H. Terrones and D. Díaz, *Small*, 2006, **2**, 346-350.
25. J. Yuan and M. Antonietti, *Macromolecules*, 2011, **44**, 744-750.
26. J. Yuan, C. Giordano and M. Antonietti, *Chem. Mater.*, 2010, **22**, 5003-5012.
27. J. Yuan, A. G. Márquez, J. Reinacher, C. Giordano, J. Janek and M. Antonietti, *Polym. Chem.*, 2011, **2**, 1654-1657.
28. J. Yuan, H. Schlaad, C. Giordano and M. Antonietti, *Polym. Chem.*, 2011, **47**, 772-781.
29. X. Bo, J. Bai, J. Ju and L. Guo, *J. Power Sources*, 2011, **196**, 8360-8365.
30. J. Yuan, S. Soll, M. Drechsler, A. H. Müller and M. Antonietti, *J. Am. Chem. Soc.*, 2011, **133**, 17556-17559.
31. M. R. Nabid and S. J. Tabatabaei Rezaei, *Appl. Catal. A: Gen.*, 2009, **366**, 108-113.
32. M. R. Nabid, Y. Bide, N. Ghalavand and M. Niknezhad, *Appl. Organomet. Chem.*, 2014, **28**, 389-395.
33. M. R. Nabid, Y. Bide, E. Aghaghafari and S. Rezaei, *Catal Lett*, 2014, **144**, 355-363.
34. M. R. Nabid and Y. Bide, *Appl. Catal. A: Gen.*, 2014, **469**, 183-190.
35. M. R. Nabid, Y. Bide and M. Abuali, *RSC Adv.*, 2014, **4**, 35844-35851.
36. M. R. Nabid, Y. Bide and S. J. Tabatabaei Rezaei, *Appl. Catal. A: Gen.*, 2011, **406**, 124-132.
37. M. R. Nabid, Y. Bide and M. Niknezhad, *ChemCatChem*, 2014, **6**, 538-546.
38. F. Alonso, P. Riente and M. Yus, *Tetrahedron*, 2008, **64**, 1847-1852.
39. T. Li, W. Zhang, R. Z. Lee and Q. Zhong, *Food Chem.*, 2009, **114**, 447-452.
40. M. J. Gracia, J. M. Campelo, E. Losada, R. Luque, J. M. Marinas and A. A. Romero, *Org. Biomol. Chem.*, 2009, **7**, 4821-4824.
41. L. Znak and J. Zieliński, *Appl. Catal. A: Gen.*, 2008, **334**, 268-276.
42. V. B. Parambath, R. Nagar and S. Ramaprabhu, *Langmuir*, 2012, **28**, 7826-7833.
43. G. Socrates, *Infrared and Raman characteristic group frequencies: tables and charts*, John Wiley & Sons, 2004.
44. H. Blaser, A. Baiker and R. Prins, *Heterogeneous catalysis and fine chemicals IV*, Elsevier, 1997.
45. T.-P. Fellingner, A. Thomas, J. Yuan and M. Antonietti, *Adv. Mater.*, 2013, **25**, 5838-5855.
46. O. Metin and S. Ozkar, *Energy & Fuels*, 2009, **23**, 3517-3526.
47. E. Paleček, M. Bartošík, V. Ostatná and M. Trefulka, *Chem. Rec.*, 2012, **12**, 27-45.
48. D. W. Himmelberger, C. W. Yoon, M. E. Bluhm, P. J. Carroll and L. G. Sneddon, *J. Am. Chem. Soc.*, 2009, **131**, 14101-14110.
49. A. Levy, J. B. Brown and C. J. Lyons, *Ind. Eng. Chem. Res.*, 1960, **52**, 211-214.
50. B. H. Liu, Z. P. Li and S. Suda, *J. Alloys Compd.*, 2006, **415**, 288-293.
51. A. Gutowska, L. Li, Y. Shin, C. M. Wang, X. S. Li, J. C. Linehan, R. S. Smith, B. D. Kay, B. Schmid and W. Shaw, *Angew. Chem. Int. Ed.*, 2005, **44**, 3578-3582.
52. C. W. Jones, *Top. Catal.*, 2010, **53**, 942-952.
53. J. Wang, Y. Li, P. Li and G. Song, *Monatsh. Chem.*, 2013, **144**, 1159-1163.
54. J. Liu, Z. Sun, Y. Deng, Y. Zou, C. Li, X. Guo, L. Xiong, Y. Gao, F. Li and D. Zhao, *Angew. Chem. Int. Ed.*, 2009, **48**, 5875-5879.